

# The ultraviolet continuum slopes ( $\beta$ ) of galaxies at $z \simeq 8 - 15$ from JWST and ground-based near-infrared imaging

Fergus Cullen<sup>1\*</sup>, R. J. McLure<sup>1</sup>, D. J. McLeod<sup>1</sup>, J. S. Dunlop<sup>1</sup>, C. T. Donnan<sup>1</sup>, A. C. Carnall<sup>1</sup>,  
R. A. A. Bowler<sup>2</sup>, R. Begley<sup>1</sup>, M. L. Hamadouche<sup>1</sup>

<sup>1</sup>*Institute for Astronomy, University of Edinburgh, Royal Observatory, Edinburgh, EH9 3HJ, UK*

<sup>2</sup>*Jodrell Bank Centre for Astrophysics, University of Manchester, Oxford Road, Manchester, M13 9PL, UK*

Accepted XXX. Received YYY; in original form ZZZ

## ABSTRACT

We study the rest-frame ultraviolet (UV) continuum slopes ( $\beta$ ) of galaxies at redshifts  $8 < z < 15$ , using a combination of *James Webb Space Telescope* (JWST) ERO and ERS NIRcam imaging and ground-based near-infrared imaging of the COSMOS field. The combination of JWST and ground-based imaging provides a wide baseline in both redshift and absolute UV magnitude ( $-22.5 < M_{\text{UV}} < 18.5$ ), sufficient to allow a meaningful comparison to previous results at lower redshift. Using a power-law fitting technique, we find that our full sample (median  $M_{\text{UV}} = -19.5 \pm 1.1$ ) returns an inverse-variance weighted mean value of  $\langle \beta \rangle = -2.07 \pm 0.05$ , with a corresponding median value of  $\beta = -2.26 \pm 0.12$ . These values imply that the UV colours of galaxies at  $z > 8$  are, *on average*, no bluer than the bluest galaxies in the local Universe. Moreover, we find tentative evidence for a  $\beta - M_{\text{UV}}$  relation, such that brighter UV galaxies display somewhat redder UV slopes ( $d\beta/dM_{\text{UV}} = -0.12 \pm 0.05$ ). Comparing to results at lower redshift, we find that the slope of our  $\beta - M_{\text{UV}}$  relation is fully consistent with that observed at  $z \simeq 5$  and that, at a given  $M_{\text{UV}}$ , our  $8 < z < 15$  galaxies are somewhat bluer ( $\delta\beta = -0.27 \pm 0.06$ ) than their  $z \simeq 5$  counterparts. Finally, we do not find strong evidence that any objects in our sample display ultra-blue UV continuum slopes (i.e.,  $\beta \lesssim -3$ ) that would require their UV emission to be dominated by ultra-young, dust-free stellar populations with high Lyman-continuum escape fractions.

**Key words:** galaxies: evolution - galaxies: formation - galaxies: high-redshift - galaxies: starburst - dark ages, reionization, first stars

## 1 INTRODUCTION

Constraining the physical properties of the first galaxies is a key goal of the *James Webb Space Telescope* (JWST). Within the first month of the data being released, JWST has already revealed a substantial population of previously unseen galaxies at  $z > 10$  (e.g., Atek et al. 2022; Castellano et al. 2022; Naidu et al. 2022; Donnan et al. 2022; Finkelstein et al. 2022; Harikane et al. 2022), as well as one galaxy candidate at  $z \simeq 17$  (within  $\approx 200$  Myr of the Big Bang; Donnan et al. 2022). These galaxies provide an unprecedented opportunity to study the properties of primordial stellar populations in the early Universe.

One potential indicator of ultra-young, ultra-low metallicity, stellar populations is the power-law index of the rest-frame ultraviolet (UV) continuum,  $\beta$ , where  $f_{\lambda} \propto \lambda^{\beta}$ . At very young ages and low metallicities (e.g.,  $t < 30$  Myr and  $Z_{\star} \lesssim 10^{-3}$ ), and in the absence of dust extinction and nebular continuum emission, a very low (i.e., blue) value of  $\beta \simeq -3$  is expected (e.g., Schaerer 2002; Bouwens et al. 2010). A robust determination of  $\beta = -3$  would unequivocally indicate a stellar population that has recently formed from pristine (or near-pristine) gas with a large ionizing photon escape fraction (e.g., Robertson et al. 2010). Finding such galaxies would therefore have crucial implications for our understanding of the first galaxies and the process of cosmic hydrogen reionization.

In the pre-JWST era, no strong evidence for such primordial  $\beta = -3$  populations was found. Studies of faint galaxies up to  $z \simeq 7-8$

with the *Hubble Space Telescope* (HST) revealed an average power-law index of  $\langle \beta \rangle \simeq -2$ , indicating moderately young and metal-poor, but in no sense extreme, stellar populations (e.g., Dunlop et al. 2013; Finkelstein et al. 2012; Bouwens et al. 2014). Indeed,  $\beta \simeq -2$  is typical of the bluest galaxies observed at  $z \simeq 2-4$  (e.g., McLure et al. 2018), and even in the local Universe (e.g., NGC 1703,  $\beta = -2.3$ ; Calzetti et al. 1994). Instructively, early claims of extremely blue (i.e.,  $\beta \simeq -3$ ) galaxies from HST imaging were later shown to be the result of an observational bias, pushing measurements towards artificially blue  $\beta$  values for faint sources near the detection threshold (Bouwens et al. 2010; Dunlop et al. 2012; Rogers et al. 2013).

By providing unprecedentedly deep infrared imaging up to  $\lambda = 5 \mu\text{m}$ , JWST/NIRCam now enables the first robust estimates of  $\beta$  for galaxies at  $z > 8$ . Recently, Topping et al. (2022) have provided the first measurements of  $\beta$  at  $z \simeq 7-11$  from JWST/NIRCam imaging in the EGS field. They find a median value of  $\beta = -2.1$ , consistent with the moderately blue, but otherwise unremarkable, populations found with HST. Interestingly, however, Topping et al. (2022) also report three galaxies with seemingly secure  $\beta \simeq -3$  measurements. The ultra-blue UV slopes inferred for these sources are bolstered by a lack of nebular emission-line signatures in the rest-frame optical photometry, indicating the large ionizing photon escape fractions expected for such a population.

In this letter we use the new galaxy sample described in Donnan et al. (2022) to present a complementary study of UV continuum slopes for  $N = 53$  galaxies in the redshift range  $z \simeq 8-15$  (with mean  $\langle z \rangle \simeq 10$ ). The Donnan et al. (2022) sample combines galaxies drawn from the early JWST deep fields (at  $z \simeq 8-15$ ) with an additional sample selected from wide-area ground-based near-IR

\* E-mail: fc@roe.ac.uk

imaging in the COSMOS/UltraVISTA field (at  $z \approx 8 - 10$ ). Crucially, with the inclusion of this ground-based sample, we can also probe the brightest galaxies at these redshifts, which evade current JWST surveys. This extended baseline in UV luminosity enables us to investigate  $\beta$  across a factor of  $\approx 40$  in UV luminosity, placing early constraints on the relationship between  $\beta$  and UV magnitude at  $z > 8$  (i.e.,  $\beta - M_{\text{UV}}$  or the colour-magnitude relation; Rogers et al. 2014).

Our aim is to provide an exploratory study of the constraints on  $\beta$  at  $z > 8$  enabled by deep JWST multi-band imaging, and to critically assess any early evidence for an evolution in the typical  $\beta$  values, as well as the relation between  $\beta$  and  $M_{\text{UV}}$  at these redshifts. We also examine evidence for any robust  $\beta \approx -3$  sources in our sample, and discuss the possibility of spurious  $\beta \leq -3$  detections for faint sources in the new JWST imaging.

The paper is structured as follows. In Section 2 we describe the data and galaxy sample constructed by Donnan et al. (2022), and provide the details of our method for determining  $\beta$ . In Section 3 we present our  $\beta$  measurements and outline the main results of our analysis, before summarising our conclusions in Section 4. Throughout we use the AB magnitude system (Oke 1974; Oke & Gunn 1983), and assume a standard cosmological model with  $H_0 = 70 \text{ km s}^{-1} \text{ Mpc}^{-1}$ ,  $\Omega_m = 0.3$  and  $\Omega_\Lambda = 0.7$ .

## 2 DATA AND UV CONTINUUM SLOPE FITTING

### 2.1 JWST NIRC*am* imaging

Our JWST sample is drawn from public NIRC*am* imaging of three fields (SMACS J0723, GLASS and CEERS) released as part of the Early Release Observations (ERO, see Pontoppidan et al. 2022) and Early Release Science (ERS) programmes (Treu et al. 2022). Each of the three JWST fields were imaged in a combination of the F090W, F115W, F150W, F200W, F277W, F356W, F410M and F444W filters, with the specific combination of filters varying slightly from field to field (see Table 2 of Donnan et al. 2022). This JWST NIRC*am* imaging was reduced using PENCIL (PRIMER enhanced NIRC*am* Image Processing Library) which is a custom version of the JWST pipeline (1.6.0). The astrometry of the reduced images was aligned using SCAMP (Bertin 2006) to GAIA EDR3 and aligned and stacked to the same pixel scale of 0.031 arcsec using SWARP (Bertin 2010). The final combined JWST NIRC*am* imaging area totalled  $\approx 45 \text{ arcmin}^2$  (with some variation between filters).

Our JWST catalogues were created by running SOURCE EXTRACTOR (Bertin & Arnouts 1996) in dual-image mode with the F200W image as the detection image. This was to optimise our catalogue to select  $z \geq 8$  galaxies as this filter encompasses the bright UV flux just red-ward of the Lyman break. We used 8-pixel diameter (0.248-arcsec diameter) apertures on the imaging taken through the SW filters (F090W, F115W, F150W, F200W) and 11-pixel diameter (0.341-arcsec diameter) apertures on the LW imaging (F277W, F356W, F410M, F444W). Redshifts for each object in the catalogue were estimated using the photometric redshift fitting code EAZY (Brammer et al. 2008). A thorough selection procedure, described in Donnan et al. (2022), resulted in a final sample of 39 galaxies at  $z > 8.5$  across the three fields.

For the purposes of the present paper we recomputed the photometry for each JWST target in 16-pixel diameter (0.5-arcsec diameter) apertures. This was to prevent biases in  $\beta$  measurements for more extended sources (Rogers et al. 2014). These larger-diameter flux measurements were then corrected to 86% of total flux based on a

point-source correction derived from curves of growth determined from the imaging in each JWST NIRC*am* filter. In the process of computing the new large-aperture photometry, two sources (SMACS 9544  $z = 9.1$  and CEERS 30498  $z = 10.9$ ) became contaminated by diffuse light from a nearby low-redshift galaxy and was removed from the sample analysed here. This left a total of 37 galaxies in the JWST sample. Nevertheless, we note that the conclusions of this paper are not affected by adopting the original photometry and full sample presented in Donnan et al. (2022).

Absolute rest-frame UV magnitudes ( $M_{\text{UV}}$ ) were calculated for each object by integrating the best-fitting EAZY spectral energy distribution (SED) through a tophat filter centered on  $\lambda_{\text{rest}} = 1500 \text{ \AA}$  (Donnan et al. 2022).

### 2.2 COSMOS UltraVISTA

The COSMOS sample is drawn from the UltraVISTA survey (McCracken et al. 2012) which provides deep  $YJHK_s$  near-IR imaging across  $1.8 \text{ deg}^2$  in the COSMOS field, taken using ESO's VISTA telescope in Chile. The deep near-IR imaging is supplemented with optical imaging in  $u^*griz$  from the CFHT Legacy Survey (Hudelot et al. 2012), and the  $GRIZy+NB816+NB921$  filters from the Hyper Suprime-Cam Subaru Strategic Program (HSC-SSP) DR2 (Aihara et al. 2019). All the near-infrared and optical imaging in COSMOS was aligned to the GAIA EDR3 reference frame using SCAMP, re-sampled using SWARP to a common pixel scale of 0.15-arcsec, and homogenised to the point-spread-function of the UltraVISTA  $Y$ -band. Additionally, the ground-based datasets were further augmented by  $3.6\mu\text{m}$  and  $4.5\mu\text{m}$  photometry from *Spitzer*/IRAC imaging provided by the Cosmic Dawn Survey (Euclid Collaboration et al. 2022). The IRAC photometry was extracted using the source deconvolution software package TPHOT (Merlin et al. 2015).

Our COSMOS catalogues were then produced from inverse variance weighted stacks of the data in the  $Y$ ,  $J$ ,  $H$ , and  $K_s$ -bands as described in Donnan et al. (2022). Photometric redshifts were estimated with EAZY and, after applying a robust selection criteria, we retained a final sample of 16 galaxies at  $z > 7.5$ . Absolute rest-frame UV magnitudes were calculated for each object from the best-fitting EAZY SED. Combined, our JWST and COSMOS/UltraVISTA samples yielded a total of 53 galaxies at  $z \approx 8 - 15$ .

### 2.3 Measuring the UV continuum slope

A number of different approaches for measuring the UV continuum slope from broadband photometry have been practiced in the literature, including single colour measurements (e.g., McLure et al. 2011; Dunlop et al. 2012, 2013) and SED template fitting (e.g., Finkelstein et al. 2012). Here we have adopted a similar approach to the power-law fitting method advocated by Rogers et al. (2014) in their study of the  $\beta - M_{\text{UV}}$  relation at  $z \approx 5$ . For each source, the redshift was fixed to the best-fitting photometric redshift estimated by Donnan et al. (2022) and the photometry covering rest-frame wavelengths  $\lambda_{\text{rest}} \leq 3000 \text{ \AA}$  was modelled as a pure power law ( $f_\lambda \propto \lambda^\beta$ ), with IGM absorption at  $\lambda \leq 1216 \text{ \AA}$  included using the Inoue et al. (2014) prescription. The only free parameter in this approach is  $\beta$ , the power-law spectral index of the UV continuum red-ward of  $\lambda = 1216 \text{ \AA}$ . We allowed  $\beta$  to vary over the range  $-10 \leq \beta \leq 10$  and used the nested sampling code *dynesty* (Speagle 2020) to sample the full posterior distribution assuming a uniform prior.

Our approach is similar to the power-law fitting method used by Topping et al. (2022), with the main difference being that our IGM

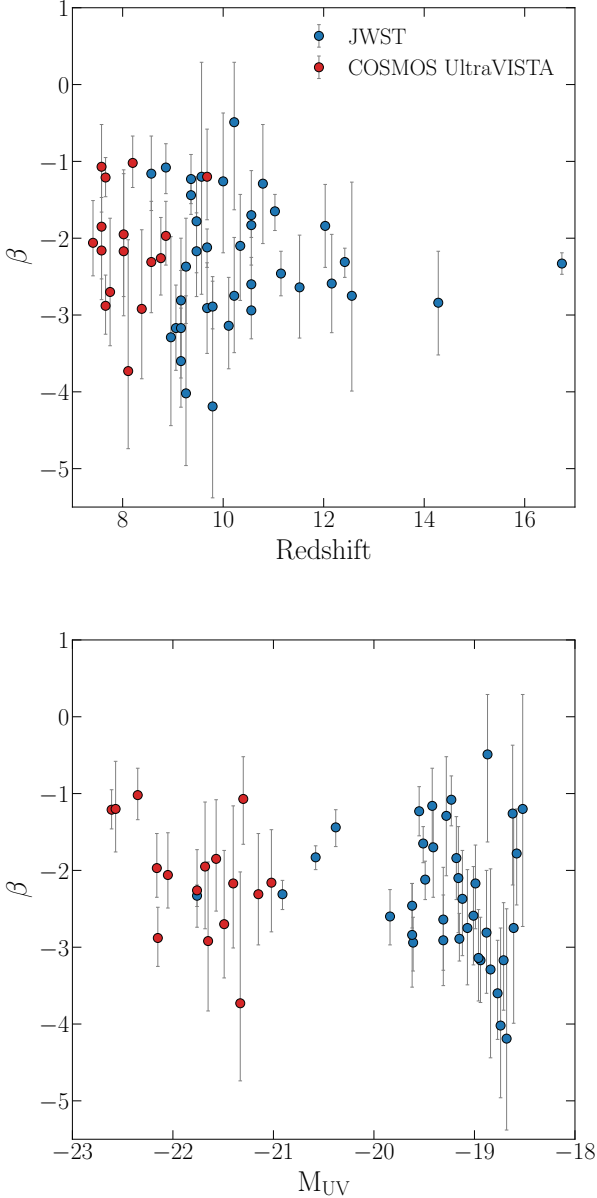


**Figure 1.** Plots of UV continuum slope  $\beta$  versus redshift (top) and versus absolute magnitude  $M_{UV}$  (bottom) for the galaxies in our JWST (blue) and COSMOS/UltraVISTA (red) sub-samples.

model enables us to include filters encompassing the Lyman break. However, our results are unchanged if we restrict the fitting to filters red-ward of 1216 Å. Finally, it is worth noting that we have explicitly assumed that any nebular emission lines present in the UV spectrum have a negligible impact on the observed photometry.

### 3 RESULTS

In Fig. 1 we plot the  $\beta$  values for our full JWST and COSMOS/UltraVISTA sample versus redshift,  $z$ , and absolute UV magnitude,  $M_{UV}$ . As well as illustrating the typical  $\beta$  values in our sample, the plots clearly demonstrate the power of combining JWST with ground-based surveys to probe a large dynamic range in both  $z$  and, particularly,  $M_{UV}$ . The first point to note is the large scatter in ob-

**Table 1.** Average  $\beta$  values and standard errors derived for our full sample in two bins of absolute UV magnitude. The first column defines each sample in terms of  $M_{UV}$ . In the second column we report the inverse-variance weighted mean and standard error of the individual  $\beta$  values. In the third column we report the median and  $\sigma_{MAD}$  of the individual  $M_{UV}$  values, where  $\sigma_{MAD} = 1.483 \times MAD$  and  $MAD$  refers to the median absolute deviation.

Sample	$\langle\beta\rangle$	$\langle M_{UV}\rangle$
Full sample (all $M_{UV}$ )	$-2.07 \pm 0.05$	$-19.5 \pm 1.1$
$M_{UV} \leq -20.5$	$-2.02 \pm 0.07$	$-21.7 \pm 0.6$
$M_{UV} > -20.5$	$-2.14 \pm 0.08$	$-19.1 \pm 0.4$

served  $\beta$  values, which increases towards the faint luminosity limit in both samples. This effect is seen most dramatically for the JWST sample, where values as extreme as  $\beta < -4$  are apparently seen at  $M_{UV} \gtrsim -19$ . However, the large error bars at these faint luminosities ( $\sigma_\beta \simeq 1$  at  $M_{UV} > -19$ ) suggests that this is predominantly a result of observational uncertainties. Indeed, the preference for low-luminosity galaxies to be scattered blue is a well-known effect, caused by the fact that if a galaxy’s flux is boosted into the detection band it will always be biased towards bluer UV slopes (Dunlop et al. 2013; Rogers et al. 2013). At the brightest UV luminosities in the JWST sample, where the constraints on individual  $\beta$  estimates improve significantly, the scatter noticeably reduces, and no  $\beta < -3$  objects are seen. We will discuss implications for the detection of ultra-blue objects at faint luminosities in more detail below.

In the  $\beta$  versus  $z$  plot an increase in the scatter at  $z \simeq 9 - 10$  is apparent for the JWST sample. This is caused by a combination of (i) a larger number of intrinsically faint galaxies being detected in this redshift range, and (ii) a minimum in the number of filters covering rest-frame wavelengths  $\lambda_{rest} \leq 3000$  Å (typically  $N_{\text{filt}} = 3$  at  $z \leq 10.5$  versus  $N_{\text{filt}} = 4$  at  $z \gtrsim 10.5$ , depending on the field). Interestingly, one of our most robust  $\beta$  estimates is the putative  $z \simeq 16.7$  galaxy candidate (CEERS 93316) reported in Donnan et al. (2022), which has  $\beta = -2.30 \pm 0.15$ . This tight constraint is due, in part, to the excellent sampling of the rest-frame UV slope for this galaxy (it is covered by the F277W, F356W, F410M and F444W filters). Promisingly, if these extremely high-redshift objects are confirmed - and if more are uncovered - JWST will be able to accurately constrain their UV continuum slopes thanks to the excellent coverage of the rest-frame UV continuum at  $z > 11$ .

It can be seen from Fig. 1 that the typical values of  $\beta$  displayed by the galaxies in our  $z \simeq 8 - 15$  sample are not obviously more extreme than the typical values found at  $z \leq 8$  with HST (i.e.,  $\beta \simeq -2$ ; Dunlop et al. 2013). There is no strong trend either with redshift or with  $M_{UV}$ , and the distribution of points in Fig. 1 is consistent with being drawn from an underlying population with a relatively narrow *intrinsic* distribution of  $\beta$ . In Table 1 we report the inverse-variance weighted mean  $\beta$  value for our full sample, which we find to be  $\langle\beta\rangle = -2.07 \pm 0.05$ . In this instance we preferred the weighted mean over the median so as not to be biased by the blue-scatter effect at faint luminosities (i.e., the blue-scattered galaxies are not down-weighted by their large uncertainties when taking the median). Indeed, the median of the full sample is  $\beta = -2.26 \pm 0.12$ , where the uncertainty on the median is estimated using the median absolute deviation estimator ( $\sigma_{MAD} = 1.483 \times MAD$ ). As expected, the median estimate is bluer, although the formal difference is  $< 2\sigma$ . Our median value is in good agreement with the median values reported at  $z \simeq 7 - 11$  in Topping et al. (2022) ( $\beta = -2.15$  at  $z \simeq 7$  and  $\beta = -2.10$  at  $z \simeq 8 - 11$ ).

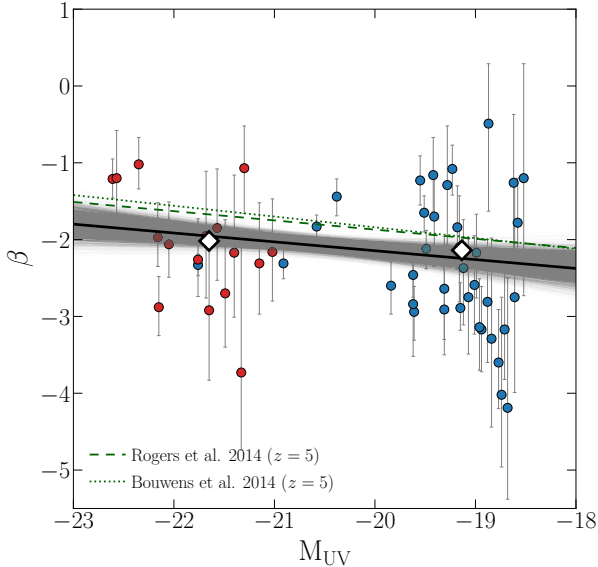


**Figure 2.** A comparison between the  $\beta$  versus  $M_{\text{UV}}$  relation at  $z > 8$  and previously-determined relations at lower redshift. The black solid line shows the best-fitting  $\beta - M_{\text{UV}}$  relation for our full sample which has a slope of  $d\beta/dM_{\text{UV}} = -0.12 \pm 0.05$ . The light-grey shaded region represents individual draws from the full posterior distribution highlighting the uncertainty on our best-fitting relation. The large diamond points are the inverse-variance weighted mean values of  $\beta$  in the two bins of absolute UV magnitude given in Table 1. The green dashed and dotted lines show the  $z \approx 5$  relations from Rogers et al. (2014) and Bouwens et al. (2014) which have  $d\beta/dM_{\text{UV}} = -0.12 \pm 0.02$  and  $d\beta/dM_{\text{UV}} = -0.14 \pm 0.02$ , respectively.

Adopting either the inverse-variance weighted mean or median, it is clear that our sample shows no evidence for significant evolution in  $\beta$  at  $z > 8$ . In fact, these early results imply that even the faintest galaxies that JWST has so far uncovered at  $z \approx 8 - 15$  have, *on average*, UV colours no more extreme than the bluest galaxies in the local Universe (e.g., NGC 1703;  $\beta = -2.3$ )

### 3.1 The colour-magnitude relation at $z > 8$

The  $\beta - M_{\text{UV}}$  relation, often referred to as the colour-magnitude relation, encodes information on the dust and stellar population properties of galaxies as a function of their absolute UV magnitude. A number of studies at  $z \lesssim 8$  have found strong evidence for a  $\beta - M_{\text{UV}}$  relation in which the UV continuum slopes of galaxies are bluer at fainter luminosities. This relationship implies that UV-faint galaxies are typically younger, less metal-enriched, and less dust-obscured than their brighter counterparts (e.g., Bouwens et al. 2014; Rogers et al. 2014).

Given the large dynamic range in  $M_{\text{UV}}$  provided by our combined JWST and COSMOS/UltraVISTA sample, we can examine early evidence for a  $\beta - M_{\text{UV}}$  relation at  $z > 8$ . In Table 1, we report the average  $\beta$  values for our sample split into two magnitude bins divided at  $M_{\text{UV}} = -20.5$ . We find  $\langle \beta \rangle = -2.14 \pm 0.08$  for the faint bin (median  $M_{\text{UV}} = -19.1$ ) and  $\langle \beta \rangle = -2.02 \pm 0.07$  for the bright bin (median  $M_{\text{UV}} = -21.7$ ). Formally, our sample is consistent with previous studies, with an evolution to redder colours in bright galaxies, although the significance is low.

Comparing our data to colour-magnitude relations derived at lower redshift, we find that the  $\beta - M_{\text{UV}}$  slope of our sample is consis-

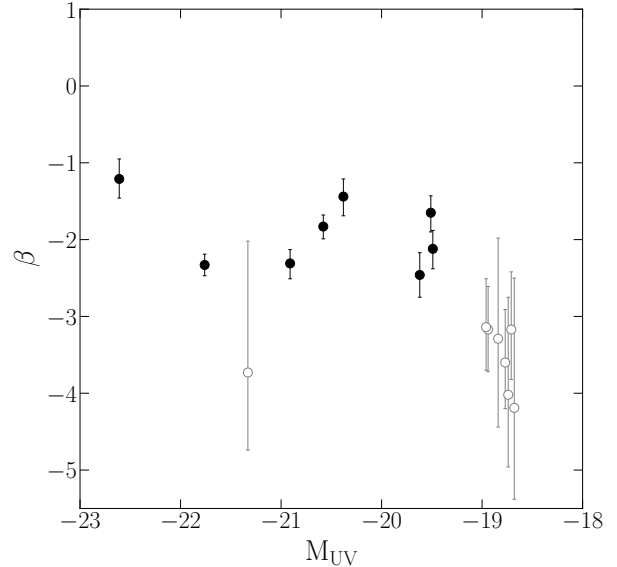


**Figure 3.** Plot of  $\beta$  versus  $M_{\text{UV}}$  for the objects with well constrained UV continuum slopes ( $\sigma_\beta < 0.3$ ; black filled circles) and the objects with  $\beta \leq -3$  (grey open circles). We find no strong evidence for UV slopes as blue as  $\beta \leq -3$  amongst those galaxies with robust measurements of  $\beta$ . All of the objects with formal  $\beta \leq -3$  solutions are poorly constrained and consistent with the known blue bias in the  $\beta$  scatter near the source detection threshold.

tent with previous determinations. In Fig. 2 we plot the  $\beta - M_{\text{UV}}$  relations at  $z \approx 5$  from Rogers et al. (2014) and Bouwens et al. (2014), who both report a modest evolution in  $\beta$  as a function of absolute UV magnitude, with  $d\beta/dM_{\text{UV}} = -0.12 \pm 0.02$  and with  $d\beta/dM_{\text{UV}} = -0.14 \pm 0.02$ , respectively. Fitting a similar colour-magnitude relation to our individual sources yields a best-fitting slope of  $d\beta/dM_{\text{UV}} = -0.12 \pm 0.05$  (black solid line in Fig. 2). It is interesting that the preliminary result from our current sample is fully consistent with the slope at  $z \approx 5$ . The data also suggest that the normalisation has evolved compared to the  $z \approx 5$  relation, with an offset of  $\delta\beta = -0.27 \pm 0.06$  at all  $M_{\text{UV}}$ .

Evidence for a signal in these early datasets is encouraging, and future larger-area JWST surveys such as PRIMER (GO 1837) will clarify this situation in the near future. These upcoming surveys will serve to both increase the sample size and fill the current magnitude gap at  $-21 < M_{\text{UV}} < -20$ . Overall, however, this comparison further emphasises the main result of our analysis: *on average*, the UV colours of our  $z \approx 8 - 15$  galaxy sample are not dramatically bluer than typical stellar populations at lower redshift.

### 3.2 Evidence for ultra-blue objects ( $\beta \approx -3$ )?

Although the typical UV slopes appear to be no bluer than the bluest galaxies observed locally, there is a known intrinsic scatter in the  $\beta$  distribution (Rogers et al. 2014), and ultra-blue objects (i.e.,  $\beta \leq -3$ ) may still exist within the population. Indeed, Topping et al. (2022) have recently identified three faint ( $M_{\text{UV}} \gtrsim -19.5$ ) sources with a reportedly secure detection of  $\beta \approx -3$  ( $\sigma_\beta \leq 0.3$ ) from their investigation of the early CEERS NIRCcam imaging data.

Our initial JWST and COSMOS/UltraVISTA sample shows no convincing evidence for such objects. It can be seen in Fig. 3 that all of the galaxies in our sample with formal best fits of  $\beta \leq -3$  have

large uncertainties in the measurement of  $\beta$ . In this case it is therefore more likely that the galaxies have been scattered to blue values due to the known blue-bias in the  $\beta$  scatter at faint luminosities (Dunlop et al. 2012; Rogers et al. 2013). In contrast, all of the galaxies with well-constrained UV slopes, which we here define as those with an uncertainty in  $\beta$  of  $\sigma_\beta \leq 0.3$  (i.e., an  $\simeq 8 - 10\sigma$  measurement, representative of the best accuracy which current public JWST imaging can deliver at these redshifts), display  $\beta > -2.5$  (note that here we have not restricted the range of available  $\beta$  values to  $\beta > -2.5$ , as can arise from the fitting of a limited range of SED templates – e.g., Nanayakkara et al. 2022). Thus the results shown in Fig. 3 strongly suggest that the majority of ultra-blue values we see in our sample are a result of statistical, rather than physical, effects.

On the other hand, Fig. 3 also demonstrates that the currently-available JWST imaging can undoubtedly deliver well-constrained  $\beta$  measurements ( $\sigma_\beta \leq 0.3$ ) for galaxies as faint as  $M_{UV} \simeq -19.5$  at  $z > 8$ , and hence should be able to uncover robust  $\beta \simeq -3$  objects at these absolute UV magnitudes should they exist (e.g., Topping et al. 2022), despite the fact that none are found here in our current high-redshift galaxy sample. In a future study, exploiting data from upcoming, wider-area, JWST Cycle-1 imaging surveys, we intend to undertake a detailed analysis of the  $\beta - M_{UV}$  relation at  $z \geq 7$  and attempt to robustly quantify the intrinsic scatter in the  $\beta$  distribution.

## 4 CONCLUSIONS

We have attempted to measure the rest-frame ultraviolet (UV) continuum slopes ( $\beta$ ) of 53 galaxies in the redshift range  $8 < z < 15$ , using a combination of *James Webb Space Telescope* (JWST) ERO and ERS NIRcam imaging and ground-based near-infrared imaging of the COSMOS/UltraVISTA field. The primary aim of this analysis is to determine whether there is any evidence for an evolution in the typical UV colours of the new population of  $z > 8$  galaxies being uncovered by JWST. We present early estimates of the *average* values of  $\beta$  at these redshifts and, using the large dynamic range in UV luminosity enabled by the combination of JWST and ground-based imaging, we investigate evidence for a  $\beta - M_{UV}$  relation in our sample. Our main conclusions can be summarized as follows.

(i) Using a power-law fitting technique, we find that our full sample displays a weighted mean value of  $\langle \beta \rangle = -2.07 \pm 0.05$ , with a corresponding median value of  $\beta = -2.26 \pm 0.12$ . This result implies that even the faintest galaxies that JWST has so far uncovered at  $z \simeq 8 - 15$  have, on average, UV colours no more extreme than the bluest galaxies in the local Universe (e.g., NGC 1703;  $\beta = -2.3$ )

(ii) We find tentative evidence for a  $\beta - M_{UV}$  relation in our sample, such that brighter UV galaxies display somewhat redder UV slopes ( $d\beta/dM_{UV} = -0.12 \pm 0.05$ ). This value is fully consistent with the slope derived at  $z \simeq 5$  by Rogers et al. (2014) and Bouwens et al. (2014) ( $d\beta/dM_{UV} = -0.12 \pm 0.02$  and  $d\beta/dM_{UV} = -0.14 \pm 0.02$ , respectively). Moreover, compared to the these  $z \simeq 5$  relations, we find that the galaxies in our sample are only modestly bluer than their  $z \simeq 5$  counterparts ( $\delta\beta = -0.27 \pm 0.06$ ).

(iii) Examining the  $\beta$  estimates for individual galaxies in our sample, we find no strong evidence for galaxies with ultra-blue UV slopes that would indicate extreme stellar populations (i.e.,  $\beta \leq -3$ ). All of the galaxies in our sample with  $\beta \leq -3$  have significant uncertainties ( $\sigma_\beta > 0.6$ ), and appear to be consistent with the well-known blue bias in the  $\beta$  scatter for sources near to the source detection threshold.

## ACKNOWLEDGEMENTS

F. Cullen, R. J. McLure, D. J. McLeod, J. S. Dunlop, C. Donnan, R. Begley and M. L. Hamadouche, acknowledge the support of the Science and Technology Facilities Council. A. C. Carnall thanks the Leverhulme Trust for their support via a Leverhulme Early Career Fellowship. RB acknowledges support from an STFC Ernest Rutherford Fellowship [grant number ST/T003596/1].

Based on observations collected at the European Southern Observatory under ESO programme ID 179.A-2005 and 198.A-2003 and on data products produced by CALET and the Cambridge Astronomy Survey Unit on behalf of the UltraVISTA consortium.

## DATA AVAILABILITY

All JWST and HST data products are available via the Mikulski Archive for Space Telescopes (<https://mast.stsci.edu>). UltraVISTA DR5 will shortly be made available through ESO. Additional data products are available from the authors upon reasonable request.

## REFERENCES

- Aihara H., et al., 2019, *PASJ*, **71**, 114  
 Atek H., Shuntov M., Furtak L. J., Richard J., Kneib J.-P., Mahler Adi Zitrin G., McCracken Clotilde Laigle Stéphane Charlot H. J., 2022, arXiv e-prints, p. arXiv:2207.12338  
 Bertin E., 2006, in Gabriel C., Arviset C., Ponz D., Enrique S., eds, *Astronomical Society of the Pacific Conference Series Vol. 351, Astronomical Data Analysis Software and Systems XV*, p. 112  
 Bertin E., 2010, SWarp: Resampling and Co-adding FITS Images Together, *Astrophysics Source Code Library*, record ascl:1010.068 (ascl:1010.068)  
 Bertin E., Arnouts S., 1996, *A&AS*, **117**, 393  
 Bouwens R. J., et al., 2010, *ApJ*, **708**, L69  
 Bouwens R. J., et al., 2014, *ApJ*, **793**, 115  
 Brammer G. B., van Dokkum P. G., Coppi P., 2008, *ApJ*, **686**, 1503  
 Calzetti D., Kinney A. L., Storchi-Bergmann T., 1994, *ApJ*, **429**, 582  
 Castellano M., et al., 2022, arXiv e-prints, p. arXiv:2207.09436  
 Donnan C. T., et al., 2022, arXiv e-prints, p. arXiv:2207.12356  
 Dunlop J. S., McLure R. J., Robertson B. E., Ellis R. S., Stark D. P., Cirasuolo M., de Ravel L., 2012, *MNRAS*, **420**, 901  
 Dunlop J. S., et al., 2013, *MNRAS*, **432**, 3520  
 Euclid Collaboration et al., 2022, *A&A*, **658**, A126  
 Finkelstein S. L., et al., 2012, *ApJ*, **756**, 164  
 Finkelstein S. L., et al., 2022, arXiv e-prints, p. arXiv:2207.12474  
 Harikane Y., et al., 2022, arXiv e-prints, p. arXiv:2208.01612  
 Hudelot P., et al., 2012, *VizieR Online Data Catalog*, p. II/317  
 Inoue A. K., Shimizu I., Iwata I., Tanaka M., 2014, *MNRAS*, **442**, 1805  
 McCracken H. J., et al., 2012, *A&A*, **544**, A156  
 McLure R. J., et al., 2011, *MNRAS*, **418**, 2074  
 McLure R. J., et al., 2018, *MNRAS*, **476**, 3991  
 Merlin E., et al., 2015, *A&A*, **582**, A15  
 Naidu R. P., et al., 2022, arXiv e-prints, p. arXiv:2207.09434  
 Nanayakkara T., et al., 2022, arXiv e-prints, p. arXiv:2207.13860  
 Oke J. B., 1974, *ApJS*, **27**, 21  
 Oke J. B., Gunn J. E., 1983, *ApJ*, **266**, 713  
 Pontoppidan K., et al., 2022, arXiv e-prints, p. arXiv:2207.13067  
 Robertson B. E., Ellis R. S., Dunlop J. S., McLure R. J., Stark D. P., 2010, *Nature*, **468**, 49  
 Rogers A. B., McLure R. J., Dunlop J. S., 2013, *MNRAS*, **429**, 2456  
 Rogers A. B., et al., 2014, *MNRAS*, **440**, 3714  
 Schaerer D., 2002, *A&A*, **382**, 28  
 Speagle J. S., 2020, *MNRAS*, **493**, 3132  
 Topping M. W., Stark D. P., Endsley R., Plat A., Whittler L., Chen Z., Charlot S., 2022, arXiv e-prints, p. arXiv:2208.01610  
 Treu T., et al., 2022, arXiv e-prints, p. arXiv:2206.07978

This paper has been typeset from a  $\text{\TeX}/\text{\LaTeX}$  file prepared by the author.